ROYAL SOCIETY OF CHEMISTRY

PAPER

Check for updates

In vitro and *in vivo* biocompatibility assessment of chalcogenide thermoelectrics as implants†

Mingyuan Gao,‡[a] Yiping Luo,‡[bc] Wen Li,*[a] Longpo Zheng*[bc] and Yanzhong Pei [ID] *[a]

The ability of thermoelectric materials to generate electricity in response to local temperature gradients makes them a potentially promising solution for the regulation of cellular functions and reconstruction of tissues. Biocompatibility of implants is a crucial attribute for the successful integration of thermoelectric techniques in biomedical applications. This work focuses on the *in vitro* and *in vivo* evaluation of biocompatibility for 12 typical chalcogenide thermoelectrics, which are composed of biocompatible elements. Ag_2Se, $SnSe$, Bi_2Se_3, $Bi_2Te_{2.88}Se_{0.12}$ and Bi_2Te_3, each with a released ion concentration lower than 10 ppm in extracts, exhibited favorable biocompatibility, including cell viability, adhesion, and hemocompatibility, as observed in initial *in vitro* assessments. Moreover, *in vivo* biocompatibility assessment, achieved by hematological and histopathological analyses in the rat subcutaneous model, further substantiated the biocompatibility of Ag_2Se, Bi_2Se_3, and Bi_2Te_3, with each possessing superior thermoelectric performance at room temperature. This work offers robust evidence to promote Ag_2Se, Bi_2Se_3, and Bi_2Te_3 as potential thermoelectric biomaterials, establishing a foundation for their future applications in biomedicine.

1. Introduction

Based on the Seebeck and Peltier effects, thermoelectric materials enable a direct conversion between heat and electricity and have been a key focus in applications involving power generation and temperature management, respectively. As microelectronics continue to evolve, with a focus on miniaturization and portability, thermoelectric devices offer novel avenues for powering microdevices and thermal regulation.[1]

Materials with the capability to generate electricity have garnered considerable attention as potential candidates for biomedical applications. This is primarily owing to the unique interaction between the generated electricity and biological systems, which can profoundly influence cellular behavior,[2] neural signal transmission,[3] tissue regeneration processes,[4] and so on. Piezoelectric materials, which can convert mechanical stress to electricity, have found diverse practical applications in biomedicine,[5] such as ultra-sensitive biosensing technologies[6] and bone tissue regeneration.[2,7] Moreover, photoelectric materials, which are capable of transforming light energy to electrical energy, offer a reliable route for the precision control of cellular activities and neuronal discharges.[8]

Thermoelectric materials, leveraging their attribute of converting temperature differences into electric power, have potential in a wide spectrum of anticipated biomedical applications.[9] Thermoelectric microdevices have been utilized for the real-time monitoring of body temperature,[10] precise adjustment of local temperature,[11] and as a power supply for medical devices.[12] Similar to piezoelectric and photoelectric materials, the unique ability of thermoelectric materials to generate electricity from body-environment temperature differentials presents a potential possibility to modulate biological systems through direct electrical stimulation of cells and tissues. This could lead to groundbreaking therapeutic strategies for wound healing, neural stimulation, and cellular function regulation, marking a new frontier in medical innovation.

For ensuring the safe and effective application of thermoelectric materials in biomedicine, a profound understanding of their interaction with biological tissues is paramount.[8b] Biocompatibility represents a pivotal criterion in assessing the safety of materials for *in vivo* applications, and it holds special significance for thermoelectric materials. This encompasses not only the immediate cellular and tissue responses, but also long-term stability post-implantation, potential immune reactions, and interactions with bodily fluids.[13]

[a] *Interdisciplinary Materials Research Center, School of Materials Science and Engineering, Tongji Univ., 4800 Caoan Rd., Shanghai 201804, China.*
E-mail: liwen@tongji.edu.cn, yanzhong@tongji.edu.cn

[b] *Department of Orthopedics, Shanghai Tenth People's Hospital, School of Medicine, Tongji Univ., 301 Yanchang Rd., Shanghai 200072, China.*
E-mail: dr.zheng@tongji.edu.cn

[c] *Orthopedic Intelligent Minimally Invasive Diagnosis and Treatment Center, Shanghai Tenth People's Hospital, School of Medicine, Tongji Univ., 301 Yanchang Rd., Shanghai 200072, China*

† Electronic supplementary information (ESI) available. See DOI: https://doi.org/10.1039/d4tb00973h

‡ The authors equally contributed.

This journal is © The Royal Society of Chemistry 2024

J. Mater. Chem. B, 2024, **12**, 6847–6855 | **6847**

These facets collectively define the host response to foreign materials, which can impact a material's functional efficacy and patient safety. Thus, a comprehensive evaluation of the biocompatibility of thermoelectric materials is indispensable to guide their medical applications and ensure their harmonious integration within biological systems.

Chalcogenide compounds, especially selenides and tellurides,[14] have been extensively demonstrated to be promising thermoelectric materials, with extraordinary performance able to be realized by applying band and defect engineering strategies.[15] These strategies are always achieved by the manipulation of the chemical constituents.[16] Thus, taking into account the elemental prevalence in biological systems and thermoelectric performance, chalcogenide thermoelectrics, such as SnSe, Ag_2Se,[17] Cu_2Se,[18] Bi_2Se_3,[19] Te,[20] GeTe,[21] SnTe,[22] MnTe,[23] Bi_2Te_3,[24] $Bi_2Te_{2.88}Se_{0.12}$,[24] $Bi_{0.5}Sb_{1.5}Te_3$,[25] Sb_2Te_3,[25] have been comprehensively investigated to uncover their biocompatibility and its dependence on the composition.

In this work, the *in vitro* cell viability assay preliminarily indicated the considerable biocompatibility of SnSe, Ag_2Se, Bi_2Se_3, Bi_2Te_3, and $Bi_2Te_{2.88}Se_{0.12}$, which could reasonably be understood by a released ion concentration lower than 10 ppm in the extracts. Moreover, the viability and morphology of the seeded cells helped elucidate the chemical reaction between the cells and thermoelectric materials (Ag_2Se, Bi_2Se_3, Bi_2Te_3, and $Bi_2Te_{2.88}Se_{0.12}$) in terms of the spreading cell morphology and stress fiber formation. *In vivo* subcutaneous implantation in rats was conducted to further identify the biocompatibility of Ag_2Se, Bi_2Se_3, and Bi_2Te_3, providing additional confirmation of the safety of these compounds for potential biomedical applications.

2. Materials and methods

2.1 Materials synthesis

Polycrystalline SnSe, Ag_2Se, Cu_2Se, Bi_2Se_3, Te, GeTe, SnTe, MnTe, Bi_2Te_3, $Bi_2Te_{2.88}Se_{0.12}$, $Bi_{0.5}Sb_{1.5}Te_3$, and Sb_2Te_3 were synthesized by sealing stoichiometric amounts of high purity elements ($\geq$99.99%) in vacuum quartz ampoules, which were melted and quenched in cold water, and then annealed. The details of the synthesis parameters for the various thermoelectric materials are listed in Table S1 (ESI†). The obtained ingots were ground into fine powders for hot-pressing and X-ray diffraction (XRD) analysis. The dense pellets ($>$98% theoretical density) $\sim$10 mm in diameter and $\sim$1.0 mm in thickness were obtained by an induction heating hot press system at different sintering conditions (Table S1, ESI†).

2.2 Characterization

The microstructure and compositional distribution were characterized by a scanning electron microscopy (SEM) system equipped with an energy-dispersive spectrometry (EDS) unit. The electrical properties, comprising the Seebeck coefficient (S), resistivity (ρ), and Hall coefficient (R_H), were simultaneously measured within 300–400 K under a helium atmosphere. Two K type thermocouples were embedded at two sides along the radial direction of the pellets for measuring both the

temperature difference and the thermopower. The Seebeck coefficient was obtained from the slope of the thermopower *vs.* temperature differences within 0–5 K. The ρ and R_H values were measured using the van der Pauw technique under a magnetic field of 1.5 T. Thermal diffusivity (D) was measured by the laser flash technique. Thermal conductivity (κ) was estimated *via* $\kappa = dC_pD$, where d is the density measured using the mass and geometric volume of the pellets and C_p is the heat capacity estimated by the Dulong–Petit approximation with an assumption of temperature independence. The measurement uncertainties for S, ρ, R_H, and κ were about 5%.

2.3 Cell culture

NIH/3T3 (mouse fibroblasts), HUVEC (human umbilical vein endothelial cells), and BMSC (human bone marrow mesenchymal stem cells) were used to assess the cellular toxicity of the thermoelectric materials. These cell lines were procured from the Cell Repository of the Chinese Academy of Sciences, Shanghai. Their propagation was facilitated in Dulbecco's modified Eagle's medium (DMEM, Gibco, USA) and minimum essential medium α (MEMα, Gibco, USA) supplemented with 10% (v/v) fetal bovine serum (FBS, Gibco, USA) and a 1% antibiotic mix of penicillin–streptomycin (Beyotime, China). Cells were nurtured under a controlled environment at 37 °C and 5% CO_2.

2.4 CCK-8 cell viability assay

To evaluate the potential cytotoxicity of the thermoelectric materials, extracts were prepared by immersing these materials in 10% FBS-containing DMEM at 37 °C with a 5% CO_2 atmosphere for 24 h, following the guidelines outlined in ISO 10993 part 12, using a ratio of 3 cm^2 mL^{-1}.[26] The cytotoxicity against NIH/3T3, HUVEC, and BMSC cells was determined using the cell counting kit (CCK)-8 assay. A count of 1×10^4 cells per well was seeded into a 96-well plate and incubated for 24 h, then the medium was replaced with material extracts after 24 h. Subsequently, CCK-8 reagent (10% v/v in DMEM, Biosharp, China) was added, and the metabolic activity was measured at 450 nm (ELISA reader, Thermo Fisher, USA).

2.5 Direct cell viability and adhesion

Thermoelectric materials were polished to a fineness of 2000 mesh and positioned within 24-well plates. Subsequently, NIH/3T3 cells were seeded onto the materials at a density of 1×10^5 cells cm^{-2} and incubated for 24 h. The viability of the cells was evaluated using a calcein AM/PI dual-staining protocol (BestBio, China), and imaged using a Leica DM68 fluorescence microscope.

The seeded cells were incubated for 24 h, and then rinsed three times with phosphate buffer saline (PBS, pH 7.4). After fixing with 2.5% glutaraldehyde at 4 °C for 4 h, the samples underwent graded ethanol dehydration, freeze-drying, and gold sputter-coating. The adhering cells' morphology was observed by SEM.

2.6 Ionic release analysis

Ion release from the thermoelectric materials was assessed using inductively coupled plasma mass spectrometry (ICP-

6848 | *J. Mater. Chem. B*, 2024, **12**, 6847–6855

This journal is © The Royal Society of Chemistry 2024

MS). The ion concentrations in the extracts were meticulously quantified, with each sample type analyzed in triplicate for statistical consistency.

2.7 Hemocompatibility assessment

Rat whole blood (approximately 5 mL) was mixed with sodium citrate (3.8% w/v) in a 9:1 ratio to prevent coagulation. Initially, 3 mL blood was centrifuged at 3000 rpm for 15 min with the supernatant discarded. The remaining red blood cells were washed with PBS and diluted in 25 mL PBS. Red blood cell (RBC) suspensions (0.25 mL) were incubated with 0.75 mL of material extracts. Distilled water and PBS were used to prepare positive and negative controls, respectively. After 2 h suspension at room temperature, the samples were centrifuged at 3000 rpm for 5 min. The absorbance of the supernatants was measured at 570 nm (ELISA reader, Thermo Fisher, USA).

2.8 *In vivo* biocompatibility assessment

The animal study protocol was approved by the Animal Ethics Committee of Shanghai Tenth People's Hospital, Tongji University, China, and followed ARRIVE guidelines. Male Sprague–Dawley rats (150–200 g, 6 weeks old) were housed in individual cages under controlled temperature and humidity conditions with a 12-h light–dark cycle. Ag_2Se, Bi_2Se_3, and Bi_2Te_3, identified for their favorable biocompatibility through *in vitro* cytotoxicity screening, were selected for *in vivo* biocompatibility assessment. Disc-shaped thermoelectric material samples (10 mm diameter, 1 mm thickness) were implanted subcutaneously to analyze the local host responses and systemic toxicity.

The animals were anesthetized using a combination of ketamine (120 mg kg^{-1} body weight) and xylazine (16 mg kg^{-1} body weight). The surgical area was shaved and disinfected. A skin incision was made on the rat's back to create a subcutaneous pocket, followed by implants insertion and suture closure. After suturing the incisions, the rats were placed in a recovery area with controlled warmth and provided with analgesics. The rats were humanely euthanized at predetermined time points of 3, 7, and 30 days post-implantation to facilitate the retrieval of the thermoelectric implants and collect the vital organs, *i.e.*, the liver, brain, kidney, heart, spleen, and tissues near the implant sites, which were then all preserved in 10% formalin for histological analysis. The selection of these time points was strategically made to correspond with the key phases of the inflammatory response: acute inflammation, proliferation, and remodeling, respectively.

2.9 Hematological and serum biochemical analysis

Blood samples were collected from the animals using ethylenediaminetetraacetic acid (EDTA)-coated tubes *via* the standard orbital sinus blood collection technique. This procedure was meticulously carried out at three implantation time points: 3, 7, and 30 days. Complete blood counts were conducted, including red blood cells (RBC), white blood cells (WBC), hemoglobin (HGB), hematocrit (HCT), mean corpuscular volume (MCV), mean corpuscular hemoglobin (MCH), mean corpuscular hemoglobin concentration (MCHC), neutrophils, lymphocytes with other immune cells, and platelets (PLTs). The serum biochemical parameters alanine aminotransferase (ALT), aspartate aminotransferase (AST), alanine aminotransferase (ALT), albumin (ALB), γ-glutamyl transferase (GGT), total bilirubin (TBIL), blood urea nitrogen (BUN), creatinine (CR), glucose (GLU), triglycerides (TG), and cholesterol (CHO) were analyzed and compared with the control group using Ti alloy implants.

2.10 Histological analysis

Collected tissues were embedded in paraffin, sectioned at 4 μm, dewaxed in xylene, and hydrated through a series of ethanol steps. Hematoxylin and eosin (H&E) staining was performed for histopathological evaluation. Masson's trichrome staining was used to assess tissue structural changes, collagen deposition, and inflammatory response post-implantation.

2.11 Statistical analysis

All the obtained experimental results were statistically probed and are expressed as the mean ± standard deviation (SD). Differences between two independent groups were assessed using the unpaired Student's *t*-test. For comparisons across multiple groups at various time points, one-way ANOVA with the Tukey HSD *post hoc* test was employed to identify significant differences between the experimental and control groups, with significance set at $p < 0.05$.

3. Results and discussion

The powder XRD patterns for the obtained thermoelectric materials are shown in Fig. S1 (ESI†). All of the diffraction peaks could be well indexed to the corresponding crystal structures, which suggested the single phases for all the materials. In addition, SEM observations and EDS mapping analysis were carried out on their hot-pressed pellets. No precipitates were observed and the constituent elements were found to be homogeneously distributed, which further confirmed the formation of single phases (Fig. S2, ESI†). The detailed thermoelectric transport properties of all the thermoelectric materials were measured and are shown in Fig. S3 (ESI†).

In vitro cytocompatibility assays can provide crucial insights into the biocompatibility of biomaterials and aid in shaping subsequent animal and clinical trial strategies. To preliminarily evaluate the *in vitro* cytocompatibility of the thermoelectric materials, the cytotoxicity to cells cultured by the extracts was evaluated using the CCK-8 assay. In addition to the biocompatible element, the stability of the materials, determining the released ion concentration, is also a crucial factor to elucidate the biocompatibility. The released ions can modulate a wide range of cellular functions and behaviors, from gene expression and metabolic activity to cell migration and differentiation.[27] The concentration of released ions, released from the thermoelectric materials, in the extracts was quantified by ICP-MS and the corresponding results are displayed in Fig. 1.

The selenides of SnSe, Ag_2Se, and Bi_2Se_3 showed ion concentrations lower than 1 ppm for each constitute element in the extracts.
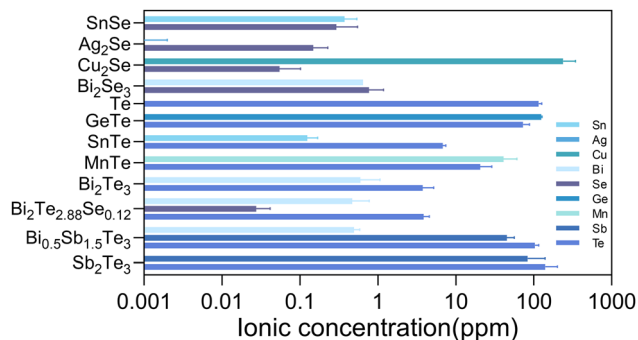
Fig. 1 Ionic concentration in the extracts of various thermoelectric materials.

Therefore, the cell viability exceeding 80% for various cells (3T3, HUVEC, and BMSC) could be reasonably understood by the low concentration of ions released (Fig. 2). According to the ISO 10993-5 biocompatibility standard, the cytotoxicity of these materials could be classified as grade 0 or 1, suggesting their considerable compatibility and a tolerable concentration range of 0.1–1 ppm for Sn, Bi, and Se. Cu_2Se was a notable exception, exhibiting diminished compatibility, associated with the substantial release of copper ions (> 100 ppm). The elevated Cu ion levels were found to interfere with essential cellular processes, including mitochondrial function and signaling pathways, culminating in apoptosis or necrosis.[28] Moreover, the Cu could catalyze the production of reactive oxygen species (ROS) through Fenton-like reactions,[29] leading to oxidative stress,[30] cellular damage, and a disruption of homeostasis.

The tellurides with the released Te ion concentration higher than 7.2 ppm in the extracts exhibited pronounced cytotoxic effects, illustrating the cytotoxicity of the 100% extracts of Te, GeTe, SnTe, MnTe, $Bi_{0.5}Sb_{1.5}Te_3$, and Sb_2Te_3. The cytotoxicity for the majority of them reached grade 4. It is known that high Te concentrations would be accompanied with irreversible oxidative stress, which would then disrupt intracellular organization and the energy balance,[31] which would be detrimental to cells. Bi_2Te_3 and $Bi_2Te_{2.88}Se_{0.12}$ were found to be biocompatible with the cells of 3T3 and HUVEC, while a pronounced cytotoxicity toward BMSC was observed for these materials.

Fibroblasts are well known for their physiological roles in matrix remodeling and wound healing.[32] NIH/3T3 cells, as fibroblast models, offer a valuable system to investigate the interaction between cells and thermoelectric materials, facilitating the assessment of a material's biocompatibility and its potential to enhance cellular functions critical for tissue repair.[33] The viability and adhesion of NIH/3T3 cells directly seeded onto the surfaces of various materials were detected by live/dead cell staining technology. Titanium alloy (Ti-6Al-4V, TC4), recognized as a benchmark for its excellent biocompatibility in biomaterials, served as a control here. After 24 h incubation, the calcein AM/propidium iodide (PI) staining results, depicted in Fig. 3, delineated the proportions of live (green) and dead (red) cells. The cell growth trends were well consistent with the results from the CCK-8 assay (Fig. 2). In detail, the cell viabilities of Bi_2Se_3, SnSe, Ag_2Se,
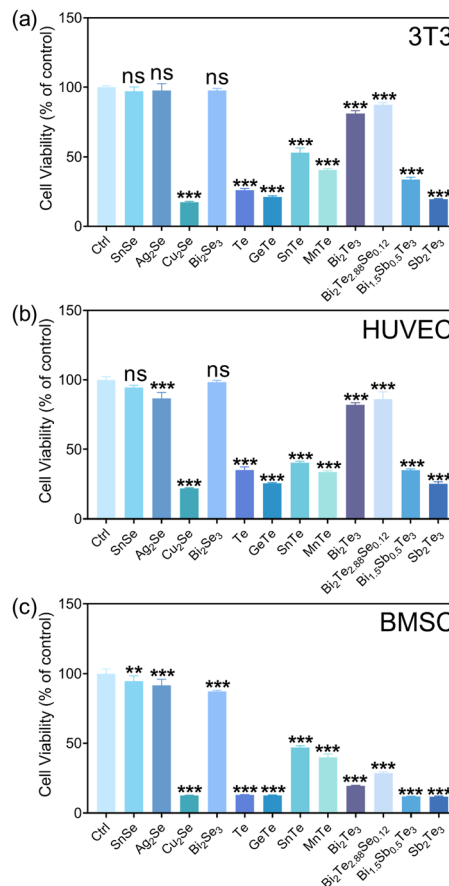

Fig. 2 Cell viability assay of various cell types of NIH/3T3 (a), HUVEC (b), and BMSC (c) after 24-hour coculture with the extracts from various thermoelectric materials. Data are presented as the mean ± s.d. ($n = 5$ biologically independent cells). Statistical differences were analyzed using Student's t-test.

$Bi_2Te_{2.88}Se_{0.12}$, and Bi_2Te_3 were qualitatively comparable to those on titanium alloy. In stark contrast, a significant reduction in cell numbers and extensive cell detachment were observed for SnTe, MnTe, and $Bi_{0.5}Sb_{1.5}Te_3$, hinting at a potential cytotoxicity. GeTe, Cu_2Se, Te, and Sb_2Te_3 exhibited a significant lack of viable NIH/3T3 cells, strongly suggesting the pronounced cytotoxic attributes of these materials. The low concentration of cells in Cu_2Se and GeTe could possibly be attributed to the dead cells being removed during the washing steps prior to staining, which could be confirmed by their poor adhesion (Fig. 4).

The morphologies of NIH/3T3 cells seeded on the thermoelectric materials after 24-h incubation were observed by SEM (Fig. 4). The NIH/3T3 cells seeded on the surfaces of Ag_2Se, Bi_2Se_3, Bi_2Te_3, and $Bi_2Te_{2.88}Se_{0.12}$ exhibited extensive spreading, characterized by a higher degree of elongation and a multitude of filopodia-like protrusions, indicative of a robust cellular engagement with the substrate. Notably, the alignment of cell adhesion morphology with the directional polishing marks on the material's surfaces suggests that microtopographical cues play a significant role in guiding cell behavior.[34] On the SnSe and $Bi_{0.5}Sb_{1.5}Te_3$ matrices, most the cells displayed effective spreading and stress fiber formation, but some

6850 | J. Mater. Chem. B, 2024, **12**, 6847–6855

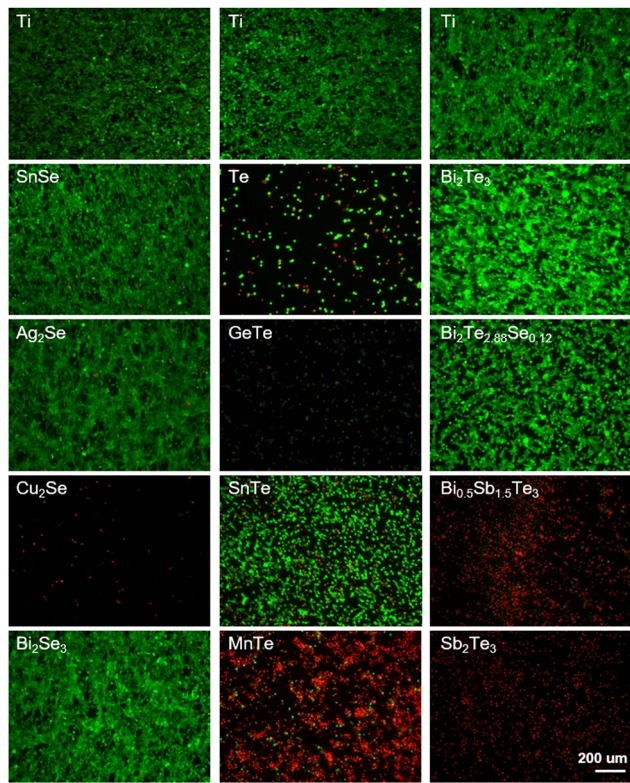This journal is © The Royal Society of Chemistry 2024

Fig. 3 Live/dead staining of NIH/3T3 cells cultured on titanium alloy (Ti) and thermoelectric materials for 24 h. Scale bar is 200 μm for all images.
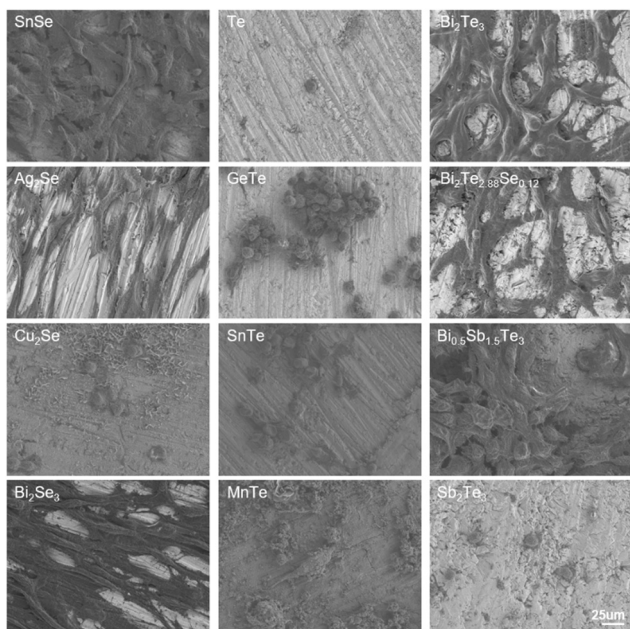

Fig. 4 SEM images of NIH/3T3 cells seeded on the surfaces of different thermoelectric materials.

presented a rounded, less adherent phenotype. In addition, the notable cellular detachment was observed on the surfaces of Cu_2Se, Te, GeTe, SnTe, MnTe, and Sb_2Te_3, along with the

remaining cells exhibiting cytoplasmic retraction and agglomeration. The observed morphological trends were consistent with the results of the cell viability. Additionally, corrosion products deposited in the form of hexagonal sheets were found on the MnTe and Cu_2Se substrates, which aligned with their high ion release as quantified in the extracts.

In the physiological environment, the release of products from thermoelectric materials into the bloodstream is inevitable. Consequently, the hemocompatibility of the thermoelectric materials was evaluated through *in vitro* hemolysis experiments (Fig. S4, ESI†). The results indicate that, with the exception of $Bi_{0.5}Sb_{1.5}Te_3$ and Sb_2Te_3, the hemolysis rates of the extracts from other thermoelectric materials were below 6% after incubation with rat whole blood, meeting the safety criteria as per ISO 10993-4 standards. This presumably originated from the existence of a high concentration of Sb in the extracts.

Based on the comprehensive consideration of the *in vitro* cytotoxicity studies and thermoelectric properties near room temperature, the *in vivo* biocompatibility of Ag_2Se, Bi_2Se_3, and Bi_2Te_3 thermoelectric materials was studied in depth by subcutaneous implantation in SD rat models, monitored meticulously over intervals of 3, 7, and 30 days. Hematological analyses revealed a minimal impact on crucial blood parameters, including red blood cells (RBC), white blood cells (WBC), hemoglobin (HGB), hematocrit (HCT), mean corpuscular volume (MCV), mean corpuscular hemoglobin (MCH), mean corpuscular hemoglobin concentration (MCHC), neutrophils, lymphocytes with other immune cells and platelets (PLT), all of which remained within the normal range, as depicted by the blue shaded area in Fig. 5. Comparative analysis with a titanium alloy control showed no significant statistical differences ($p > 0.05$), affirming their biocompatibility. The transient fluctuations in immune cell counts, including in white blood cells, suggested an initial immune response, which normalized over time, indicative of an adaptation phase to the new materials. Notably, the significant decrease in white blood cell and immune cell counts for Ag_2Se at 30 days may be related to the well-reported antibacterial properties of Ag.[35]

Furthermore, the impact of the thermoelectric materials on liver and kidney function was investigated. Comprehensive serum biochemical analyses revealed that key hepatic indicators, including albumin (ALB), alkaline phosphatase (ALP), gamma-glutamyl transferase (GGT), and total bilirubin (TBIL), remained within normal limits across all materials, as shown in Fig. 6. However, a marked deviation was observed in Ag_2Se at the 30-day mark, where the levels of alanine aminotransferase (ALT) and aspartate aminotransferase (AST) exceeded the normal range, revealing its time-dependent liver function impairment. In contrast, Bi_2Se_3 and Bi_2Te_3 exhibited mild anomalies in some parameters, albeit to a lesser extent than those of Ag_2Se, suggesting their relatively superior biocompatibility and lower chronic hepatic toxicity. Regarding renal function, all the evaluated parameters, including blood urea nitrogen (BUN) and creatinine (CREA), remained within normal ranges, signifying stable renal function without apparent renal damage throughout the study period. Additionally, the levels of blood glucose
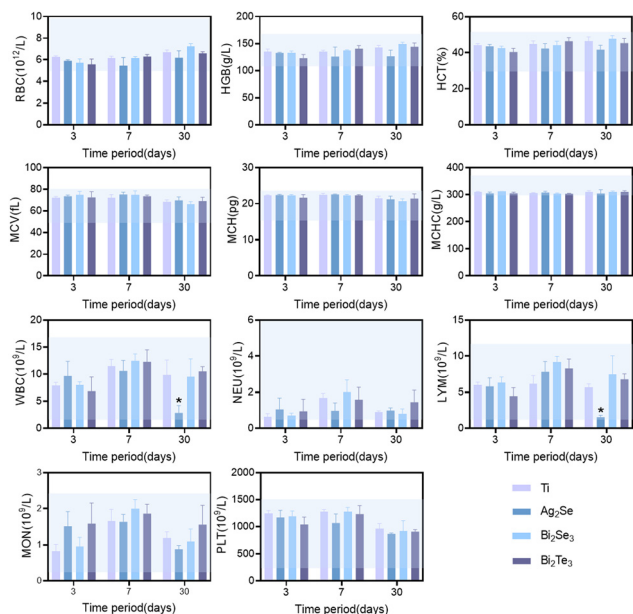
This journal is © The Royal Society of Chemistry 2024

J. Mater. Chem. B, 2024, **12**, 6847–6855 | **6851**

Fig. 5 Hematology parameters of Sprague−Dawley rats treated with thermoelectric materials at set time points. Data are presented as the mean ± s.d. ($n = 3$ biologically independent mice). * Denotes statistical significance difference at $p < 0.05$ when compared with the titanium alloy (Ti) group using ANOVA.
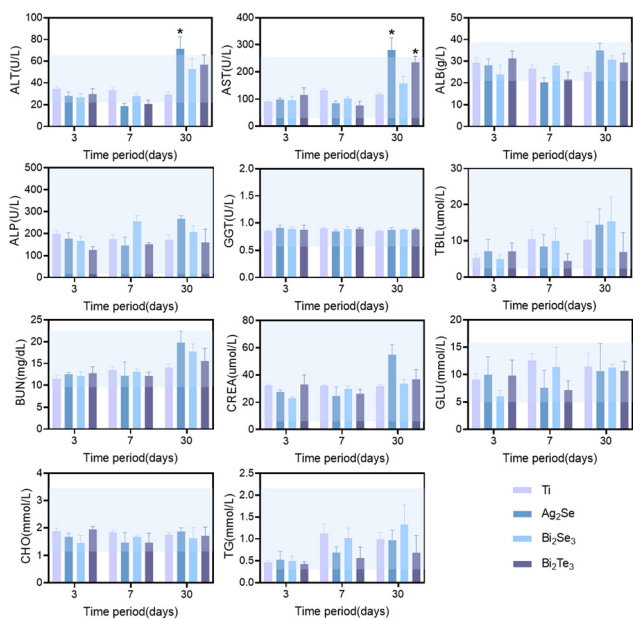

Fig. 6 Blood biochemical analysis of Sprague−Dawley rats treated with thermoelectric materials at set time points. Data are presented as the mean ± s.d. ($n = 3$ biologically independent mice). * Denotes statistical significance difference at $p < 0.05$ when compared with the titanium alloy (Ti) group using ANOVA.

and lipids were maintained within normal ranges, indicating no adverse impact on the metabolic state of the rats.

The histological response of an organ is an important indicator to evaluate the impact of implanted materials on the whole body. Hematoxylin–eosin (H&E) staining was employed to meticulously evaluate the histological soundness of various organ systems, including the heart, liver, spleen, lungs, kidneys, and brain, at different time intervals in an SD rat model (Fig. 7 and Fig. S5, S6, ESI†). The histopathological analysis revealed the absence of significant pathological modifications in these organs. Specifically, the cardiac and spleen exhibited no discernible fibrotic/necrotic alterations and a normal distribution of white and red pulp without any abnormalities, respectively. The liver could maintain its structural integrity without any indications of hepatocellular damage or inflammation. The pulmonary showed well-preserved alveolar, peribronchial, and perivascular structures, with uniform alveoli and clear bronchioles. The renal analysis displayed healthy glomeruli and tubular structures, and the brain tissues retained normal neuronal architecture and density, with no evidence of neuronal injury or edema. All these results indicate the favorable *in vivo* biocompatibility of these materials.

H&E staining was performed on the subcutaneous local tissue surrounding the implanted thermoelectric materials, as illustrated in Fig. 8. The selected time points of 3, 7, and 30 days were strategically chosen and correspond to the acute inflammatory phase, the proliferative phase, and the remodeling phase, respectively, providing a comprehensive framework to assess the materials' biocompatibility over time. All the experimental groups exhibited a consistent time-dependent increase in body weight, with no significant differences observed between groups (Fig. S7, ESI†). No macroscopic signs of rupture,
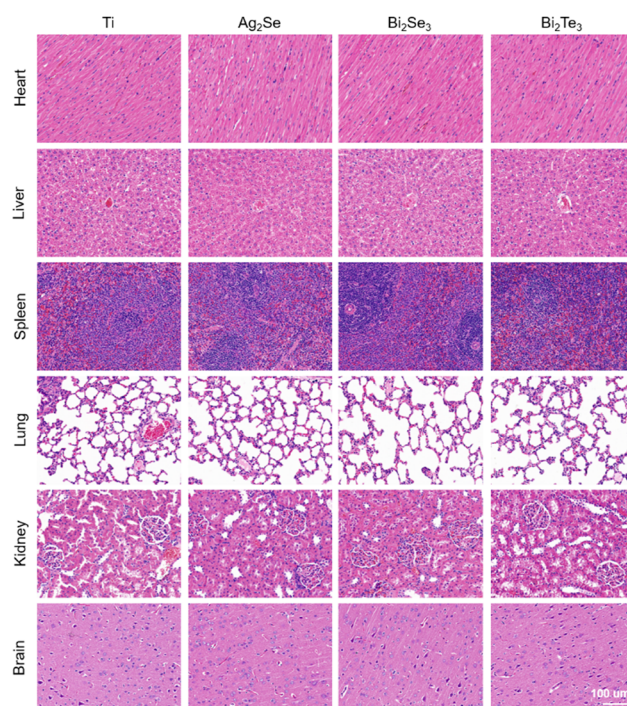

Fig. 7 Representative histological images with H&E staining of the heart, liver, spleen, lung, spleen, kidney, and brain after implantation of thermoelectric materials for 30 days ($n = 3$). The size of the scale bar corresponds to 100 μm.
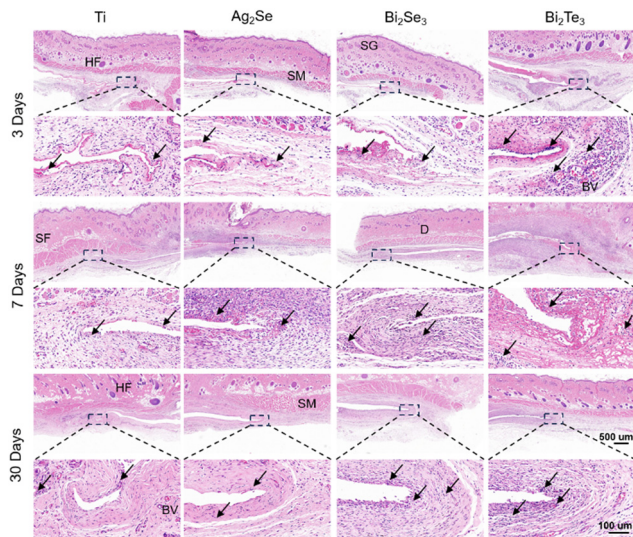
6852 | *J. Mater. Chem. B*, 2024, **12**, 6847−6855

This journal is © The Royal Society of Chemistry 2024

Fig. 8 Representative histological images of H&E staining of the subcutaneous implantation area. Unspecified black arrows, SF, HF, SG, D, SM, and BV represent inflammatory cells, subcutaneous fat, hair follicles, sebaceous glands, dermis, skeletal muscle, and blood vessels, respectively.
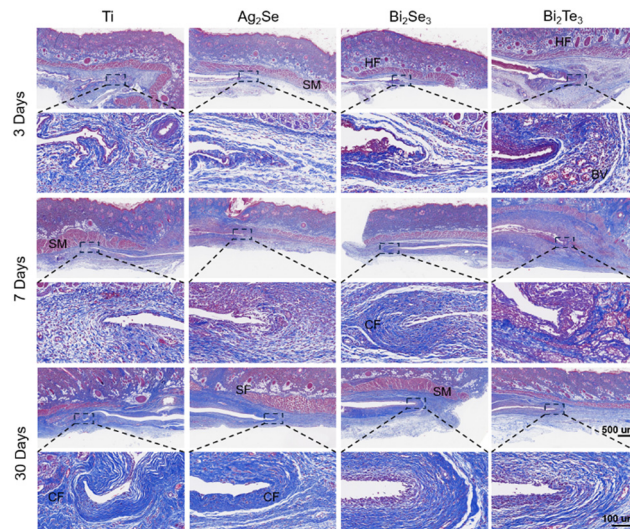

Fig. 9 Representative histological images of Masson's trichrome of the subcutaneous implantation area. Unspecified black arrows, SF, HF, SG, D, SM, BV, and CF represent inflammatory cells, subcutaneous fat, hair follicles, sebaceous glands, dermis, skeletal muscle, blood vessels, and collagenous fiber, respectively.

infection, necrosis, or edema were observed at the implantation sites (Fig. S8, ESI†). As shown in Fig. 8, all the materials initially induced a marked acute inflammatory response at the implantation sites, characterized by an aggregation of fibroblasts and inflammatory cells, including macrophages, lymphocytes, and occasional giant cells. This typical response indicated the initiation of the natural healing process and the activation of the foreign body reaction, with angiogenesis or vascular expansion observed near Bi_2Te_3 implants suggesting an intensified inflammatory stage. Over time, this reaction subsides, demonstrating effective integration between the implants and host tissue. After implanting for 30 days, a significant diminution of inflammation, particularly in the Ag_2Se group, was observed, possibly linked to the decrease in white blood cell count in the bloodstream. The formation of a thin fibrous capsule around all the materials attested to the minimal and controlled inflammatory response elicited by the materials. The variation in the thickness of the fibrous capsule (as shown in Fig. S9, ESI†) also mirrored the tissue's response and adaptation to the implanted materials, with minimal changes for Ag_2Se and the Ti control group and more pronounced variations for Bi_2Se_3 and Bi_2Te_3, indicative of the dynamic process of tissue remodeling and healing in response to the implants.

Masson's trichrome staining, as shown in Fig. 9, was used to focus on collagen deposition at the implant site (indicated by the blue stained area), a key marker for assessing tissue remodeling and healing. As the implantation period progressed, the increase in the content of collagen and restoration of fibrous structures indicated the tissue's adaptation to the materials. Particularly by day 30, the orderly arrangement of collagen fibers illustrated mature and stable tissue remodeling. These findings not only demonstrate the good tissue adaptation to the implants but also reflect the materials' biocompatibility with the surrounding

biological tissues. This is strongly related to the material stability of the material implanted (Fig. S10–S13, ESI†). Overall, these comprehensive histological analyses highlight the excellent biocompatibility and tissue integration capabilities of the studied thermoelectric materials under subcutaneous implantation conditions, providing robust scientific evidence for the potential future applications of Ag_2Se-, Bi_2Se_3-, and Bi_2Te_3-based thermoelectrics in the field of medical devices.

4. Summary

In summary, a comprehensive evaluation of biocompatibility, both *in vitro* and *in vivo*, was conducted with 12 typical chalcogenide thermoelectrics. The integration of *in vitro* cell compatibility assessments with analyses of material ion release enabled the identification of Ag_2Se, Bi_2Se_3, and Bi_2Te_3 with favorable biocompatibility profiles. This could be understood by their low released ion concentration (<10 ppm) in the extracts. Furthermore, *in vivo* biocompatibility assessment by the hematological and histopathological analyses in the rat subcutaneous model substantiated the biocompatibility of Ag_2Se, Bi_2Se_3, and Bi_2Te_3, promoting them to be potential thermoelectric biomaterials. This work lays a solid foundation for future investigations, providing valuable insights and guidance for the development and application of thermoelectric materials in the biomedical field.

Data availability

The data supporting the findings of this study are available from the corresponding author upon reasonable request.

Conflicts of interest

There are no conflicts to declare.

Acknowledgements

References

1 (a) J. Mao, G. Chen and Z. Ren, *Nat. Mater.*, 2021, **20**, 454; (b) Q. Zhang, K. Deng, L. Wilkens, H. Reith and K. Nielsch, *Nat. Electron.*, 2022, **5**, 333; (c) Z. Liu, S. Zhang, Z. Wu, E. Mu, H. Wei, Y. Liu, H. Shi and Z. Hu, *Nano Energy*, 2023, **114**, 108611.

2 G. Murillo, A. Blanquer, C. Vargas-Estevez, L. Barrios, E. Ibáñez, C. Nogués and J. Esteve, *Adv. Mater.*, 2017, **29**, 1605048.

3 Z. Liu, X. Wan, Z. L. Wang and L. Li, *Adv. Mater.*, 2021, **33**, 2007429.

4 Y. Zhang, A. Le Friec, Z. Zhang, C. A. Müller, T. Du, M. Dong, Y. Liu and M. Chen, *Mater. Today*, 2023, **70**, 237.

5 T. Vijayakanth, S. Shankar, G. Finkelstein-Zuta, S. Rencus-Lazar, S. Gilead and E. Gazit, *Chem. Soc. Rev.*, 2023, **52**, 6191.

6 D. Y. Park, D. J. Joe, D. H. Kim, H. Park, J. H. Han, C. K. Jeong, H. Park, J. G. Park, B. Joung and K. J. Lee, *Adv. Mater.*, 2017, **29**, 1702308.

7 (a) D. Khare, B. Basu and A. K. Dubey, *Biomaterials*, 2020, **258**, 120280; (b) X. Zhang, T. Wang, Z. Zhang, H. Liu, L. Li, A. Wang, J. Ouyang, T. Xie, L. Zhang, J. Xue and W. Tao, *Mater. Today*, 2023, **68**, 177.

8 (a) H. Wang, J. Tian, Y. Jiang, S. Liu, J. Zheng, N. Li, G. Wang, F. Dong, J. Chen, Y. Xie, Y. Huang, X. Cai, X. Wang, W. Xiong, H. Qi, L. Yin, Y. Wang and X. Sheng, *Sci. Adv.*, 2023, **9**, eabq7750; (b) M. Rahmati, E. A. Silva, J. E. Reseland, C. A. Heyward and H. J. Haugen, *Chem. Soc. Rev.*, 2020, **49**, 5178.

9 B. Hu, X.-L. Shi, J. Zou and Z.-G. Chen, *Chem. Eng. J.*, 2022, **437**, 135268.

10 F.-L. Gao, P. Min, Q. Ma, T. Zhang, Z.-Z. Yu, J. Shang, R.-W. Li and X. Li, *Adv. Funct. Mater.*, 2023, **34**, 2309553.

11 L. Li, W.-D. Liu, Q. Liu and Z.-G. Chen, *Adv. Funct. Mater.*, 2022, **32**, 2200548.

12 P. Bhatnagar, S. H. Zaferani, N. Rafiefard, B. Baraeinejad, A. R. Vazifeh, R. Mohammadpour, R. Ghomashchi, H. Dillersberger, D. Tham and D. Vashaee, *Prog. Mater. Sci.*, 2023, **139**, 101184.

13 S. Bauer, P. Schmuki, K. von der Mark and J. Park, *Prog. Mater. Sci.*, 2013, **58**, 261.

14 (a) L. D. Zhao, S. H. Lo, Y. Zhang, H. Sun, G. Tan, C. Uher, C. Wolverton, V. P. Dravid and M. G. Kanatzidis, *Nature*, 2014, **508**, 373; (b) Z. Zhang, K. Zhao, T.-R. Wei, P. Qiu, L. Chen and X. Shi, *Energy Environ. Sci.*, 2020, **13**, 3307; (c) H. Wu, X.-l Shi, J. Duan, Q. Liu and Z.-G. Chen, *Energy Environ. Sci.*, 2023, **16**, 1870; (d) I. T. Witting, F. Ricci, T. C. Chasapis, G. Hautier and G. J. Snyder, *Research*, 2020, **2020**, 4361703; (e) S. Lin, W. Li, Z. Chen, J. Shen,

B. Ge and Y. Pei, *Nat. Commun.*, 2016, **7**, 10287; (f) J. Li, X. Zhang, X. Wang, Z. Bu, L. Zheng, B. Zhou, F. Xiong, Y. Chen and Y. Pei, *J. Am. Chem. Soc.*, 2018, **140**, 16190; (g) J. Pei, B. Cai, H.-L. Zhuang and J.-F. Li, *Natl. Sci. Rev.*, 2020, **7**, 1856; (h) W. Li, L. Zheng, B. Ge, S. Lin, X. Zhang, Z. Chen, Y. Chang and Y. Pei, *Adv. Mater.*, 2017, **29**, 1605887; (i) Y. Luo, J. Wang, J. Yang, D. Mao, J. Cui, B. Jia, X. Liu, K. Nielsch, X. Xu and J. He, *Energy Environ. Sci.*, 2023, **16**, 3743; (j) S. I. Kim, K. H. Lee, H. A. Mun, H. S. Kim, S. W. Hwang, J. W. Roh, D. J. Yang, W. H. Shin, X. S. Li, Y. H. Lee, G. J. Snyder and S. W. Kim, *Science*, 2015, **348**, 109.

15 (a) Z. Chen, X. Zhang and Y. Pei, *Adv. Mater.*, 2018, **30**, 1705617; (b) Y. Pei, H. Wang and G. J. Snyder, *Adv. Mater.*, 2012, **24**, 6125.

16 Y. X. Wu, Z. W. Chen, P. F. Nan, F. Xiong, S. Q. Lin, X. Y. Zhang, Y. Chen, L. D. Chen, B. H. Ge and Y. Z. Pei, *Joule*, 2019, **3**, 1276.

17 L.-D. Zhao, S.-H. Lo, Y. Zhang, H. Sun, G. Tan, C. Uher, C. Wolverton, V. P. Dravid and M. G. Kanatzidis, *Nature*, 2014, **508**, 373.

18 H. Liu, X. Shi, F. Xu, L. Zhang and W. Zhang, *Nat. Mater.*, 2012, **11**, 422.

19 T. Fang, X. Li, C. Hu, Q. Zhang, J. Yang, W. Zhang, X. Zhao, D. J. Singh and T. Zhu, *Adv. Funct. Mater.*, 2019, 1900677.

20 S. Lin, W. Li, Z. Chen, J. Shen, B. Ge and Y. Pei, *Nat. Commun.*, 2016, **7**, 10287.

21 J. Li, X. Zhang, Z. Chen, S. Lin, W. Li, J. Shen, I. T. Witting, A. Faghaninia, Y. Chen, A. Jain, L. Chen, G. Jeffrey Snyder and Y. Pei, *Joule*, 2018, **2**, 976.

22 Q. Zhang, B. L. Liao, Y. C. Lan, K. Lukas, W. S. Liu, K. Esfarjani, C. Opeil, D. Broido, G. Chen and Z. F. Ren, *Proc. Natl. Acad. Sci. U. S. A.*, 2013, **110**, 13261.

23 Y. Zheng, T. Lu, M. M. H. Polash, M. Rasoulianboroujeni, N. Liu, M. E. Manley, Y. Deng, P. J. Sun, X. L. Chen, R. P. Hermann, D. Vashaee, J. P. Heremans and H. Zhao, *Sci. Adv.*, 2019, **5**, eaat9461.

24 L. Hu, H. Wu, T. Zhu, C. Fu, J. He, P. Ying and X. Zhao, *Adv. Energy Mater.*, 2015, **5**, 1500411.

25 Q. Zhang, M. Yuan, K. Pang, Y. Zhang, R. Wang, X. Tan, G. Wu, H. Hu, J. Wu, P. Sun, G.-Q. Liu and J. Jiang, *Adv. Mater.*, 2023, **35**, 2300338.

26 P. N. L. Souëf, J. Goldblatt and N. R. Lynch, *Lancet*, 2000, **356**, 242.

27 Y. Zhou, C. Wu and J. Chang, *Mater. Today*, 2019, **24**, 41.

28 M. A. Kahlson and S. J. Dixon, *Science*, 2022, **375**, 1231.

29 Y. Liu, K. Ai, X. Ji, D. Askhatova, R. Du, L. Lu and J. Shi, *J. Am. Chem. Soc.*, 2017, **139**, 856.

30 X. Wang and W. X. Wang, *Environ. Sci. Technol.*, 2023, **57**, 9548.

31 X. Ling, Z. Jin, Q. Jiang, X. Wang, B. Wei, Z. Wang, Y. Xu, T. Ca, J. W. Engle, W. Cai, C. Su and Q. He, *Natl. Sci. Rev.*, 2021, **8**, nwaa156.

32 (a) H. N. Nguyen, E. H. Noss, F. Mizoguchi, C. Huppertz, K. S. Wei, G. F. M. Watts and M. B. Brenner, *Immunity*, 2017, **46**, 220; (b) M. V. Plikus, X. Wang, S. Sinha, E. Forte,

S. M. Thompson, E. L. Herzog, R. R. Driskell, N. Rosenthal, J. Biernaskie and V. Horsley, *Cell*, 2021, **184**, 3852.

33 V. Koliaraki, A. Prados, M. Armaka and G. Kollias, *Nat. Immunol.*, 2020, **21**, 974.

34 C. J. Bettinger, R. Langer and J. T. Borenstein, *Angew. Chem., Int. Ed.*, 2009, **48**, 5406.

35 M. A. Nakvasina, I. A. Koltakov and V. G. Artyukhov, *Bull. Exp. Biol. Med.*, 2021, **170**, 499.

This journal is © The Royal Society of Chemistry 2024

J. Mater. Chem. B, 2024, **12**, 6847–6855 | **6855**